Solar Phys (2007) 242: 65–85
DOI 10.1007/s11207-007-0284-9

Helicity Patterns of the Active Regions Connected by Transequatorial Loops

Jie Chen · Shudong Bao · Hongqi Zhang

Received: 2 August 2006 / Accepted: 15 April 2007 /
Published online: 1 June 2007

Abstract Using photospheric vector magnetograms of the Huairou Solar Observing Station and coronal X-ray images from the *Yohkoh* Soft X-Ray Telescope, we calculate the helicity patterns of 43 pairs of active regions and the chirality of 50 pairs of opposite magnetic polarity regions that are connected by transequatorial loops (TLs). To make the results more convincing, two helicity proxies including the local current helicity h_c and the force-free factor α_{best} are computed. The results, which are similar for both parameters, are as follows: (1) Current helicity of the active regions pairs connected by transequatorial loops have no obvious regularity: About 50% of the active region pairs carry the same current helicity sign and about 50% of them have the opposite. (2) If we consider the magnetic polarity pairs connected by the TLs, the result is almost the same as that for the active region pairs, with a little more than half of them showing the same chirality. We also make linear force-free extrapolations for 33 TLs and determine their force-free parameter α by comparing extrapolated field lines to X-ray images of the TLs. Out of the 19 cases when the footpoints of the TLs have the same current helicity sign, we find that the sign of α of the TLs is the same as the sign of the current helicity in the footpoints in 12 cases, whereas it is of opposite sign in 4 cases, and in 3 cases the TLs were found to be potential.

1. Introduction

Transequatorial loops (TLs), which connect different regions in opposite hemispheres, have been drawn renewed attention since the launch of *Yohkoh*. It was observed that TLs may develop between existing active regions or between mature regions and new magnetic flux shortly after flux emergence (Pevtsov, 2000). The footpoints of most TLs are in moderately strong magnetic fields, but there are cases when these loops are anchored in very weak or very strong fields (Fárník, Karlický, and Švestka, 2001). Through a statistical study, Chen, Bao, and Zhang (2006) found that TLs more probably connect to the preceding polarities

J. Chen (✉) · S. Bao · H. Zhang
National Astronomical Observatories, Chinese Academy of Sciences, Beijing 100012, China
e-mail: chenjie@bao.ac.cn

than to the following polarities. Some transequatorial loops exhibit an 'S' shape or an inverse 'S' shape (Pevtsov, 2000).

The sign of the current helicity of active regions was first studied by Seehafer (1990) by comparing a variety of images with magnetograms extrapolated by assuming a constant-α force-free field. For all but two of the 16 active regions, he found negative helicity in the northern hemisphere and positive in the southern hemisphere. Later, many people (Pevtsov, Canfield, and Metcalf, 1995; Abramenko, Wang, and Yurchyshyn, 1996; Bao and Zhang, 1998; Hagino and Sakurai, 2004) researched the helicity patterns of active regions in the photosphere using vector magnetograms. Two methods can be used to calculate the chirality of the active regions from vector magnetograms: Pevtsov, Canfield, and Metcalf (1995) introduced the force-free factor α; Abramenko, Wang, and Yurchyshyn (1996) calculated the longitudinal fraction of current helicity. Both methods established the conclusion that the sign of the helicity is dependent on hemisphere.

Canfield, Pevtsov, and McClymont (1996) found that the handedness of the active regions is important in the formation of TLs. They searched the 1991 – 1995 *Yohkoh* Soft X-Ray Telescope (SXT) database and analyzed 27 pairs of regions that were close in longitude, but on opposite sites of the equator. It was found that out of these 27 pairs of active regions 17 formed transequatorial loops. Out of these 17 pairs, 15 pairs of TL footpoint regions had the same chirality. Using two cases Fárník, Karlický, and Švestka (1999) verified the result that only field lines of even more distant active regions having the same chirality reconnect. Pevtsov (2000) calculated 22 pairs of active regions connected by TLs. In 15 cases (68%) both regions had the same chirality, and in seven cases (32%) the regions had opposite chirality.

Yohkoh's superior image demonstrates solar coronal structures distinctly; some of them are simple loops or loop arcades and others exhibit an 'S' or reverse 'S' form (see, *e.g.*, Rust and Kumar, 1996). Transequatorial loops may be planar (potential) or exhibit a forward or inverse 'S' shape. We cannot determine with assurance whether a loop is potential or nonpotential from just its configuration; therefore, the definite twist signs cannot be obtained only through observing the structures of TLs. Based on force-free field extrapolation, Fárník, Karlický, and Švestka (1999) obtained the twist signs of two transequatorial loops. They also calculated the helicity signs of active regions connected by TLs and found that the signs of extrapolated TLs are the same as active regions chirality.

Transequatorial loops do not connect the total areas of active regions, but they connect part of them. Being magnetic loops, TLs connect opposite polarity regions. Generally, an active region has two main magnetic polarities. We regard the magnetic footpoint of a TL as belonging to the entire polarity region to which it appears to connect and refer to it as the *magnetic polarity region*.

In this paper, a large database covering the whole period of *Yohkoh* from the beginning (October 1991) to its end (December 2001) is considered to clarify the chirality relationship of the region pairs connected by TLs. First, the handedness of active region pairs connected by TLs are calculated, then the helicity of the magnetic polarity region pairs are analyzed. Thus, we can understand the handedness correlation of the magnetic field, which has an accurate relation to TLs. Transequatorial loops represent large-scale structures, whereas active regions and magnetic polarity regions show small-scale configurations. What about the relationship between the twist of TLs and the helicity patterns of their adjacent footpoints? To answer this question, force-free field extrapolations are made to these TLs first, then we survey the relationship of the helicity patterns between TLs and their footpoints regions.

2. Observations and Data Reduction

The whole data set of the transequatorial loops identified by Chen, Bao, and Zhang (2006) is considered in this study. Not all of the TLs connect two active regions; some of them may be anchored in quiet regions. Through co-aligning the full-disk longitudinal magnetograms (obtained from SOHO/MDI or the National Solar Observatory at Kitt Peak) and soft X-ray images, the TLs connecting two active regions are selected. Then we investigate the vector magnetogram data set of the Huairou Solar Observing Station (HSOS).

2.1. Vector Magnetic Field Data Reduction

2.1.1. Observational Technique

Vector magnetograms in the photosphere were obtained by the Solar Magnetic Field Telescope, an imaging vector magnetograph (Ai and Hu, 1986) installed at HSOS, with a field of view of about $5'.23 \times 3'.63$ (512×512 pixels of the CCD). We deduce the vector magnetic fields on the basis of four Stokes parameters I, Q, U, and V. The longitudinal component of the magnetic field (parameter V) was measured at 0.075 Å from the line center of Fe I λ5324.19 Å, and the transverse components (Q and U) were measured at the line center. Each magnetogram used in this paper is the sum of 256 individual frames for both line-of-sight and transverse fields. The temporal resolution is about 5 min and the spatial resolution is 2×2 arcsec after a smoothing average of 4×3 pixels to the Stokes parameters Q, U, and V for each magnetogram. The relation between the magnetic field and Stokes parameters are established as follows:

$$B_{\parallel} = C_{\parallel} \frac{V}{I}, \tag{1}$$

$$B_{\perp} = C_{\perp} \left(\frac{Q^2}{I^2} + \frac{U^2}{I^2} \right)^{\frac{1}{4}}, \tag{2}$$

where $C_{\parallel}$ and $C_{\perp}$ are the calibration coefficients for line-of-sight and transverse components of the magnetic field. Both theoretical and empirical methods are used to calibrate the vector magnetograms (Ai, Li, and Zhang, 1982; Wang, Ai, and Deng, 1996). The 180° azimuthal ambiguity in determining the transverse field direction is an intrinsic defect of the Zeeman effect, and it is resolved according to the potential field approximation method (Wang, Xu, and Zhang, 1994). West and Hagyard (1983) showed that the azimuth of the transverse field can be rotated when the filter setting is changed from the center to the far wing. The transverse magnetic field at Huairou were measured near the line center, which makes it necessary to correct for Faraday rotation. We correct it according to a nonlinear least-squares fitting method (Su and Zhang, 2004), which can be described by the equation (J. Su, private communication)

$$\overline{\Delta\phi} = 0.412 + 0.015 B_z. \tag{3}$$

$\overline{\Delta\phi}$ is the mean value of maximum Faraday rotation. There is a positive difference in azimuths for positive longitudinal field and a negative difference for a negative field (Landi Degl'Innocenti, 1979; Sakurai, 2001), which means that $|\overline{\Delta\phi}|$ is subtracted for a positive field and added for a negative one. However, this equation will not work correctly for pixels with very strong magnetic field that exhibit magnetic saturation. Given the small number of

such pixels, the results of this study will not be affected. The noise level in all the line-of-sight magnetograms is $\leq$20 G; taking into account the correction of Faraday rotation, we only use the data that are greater than 30 G. For the transverse field measurements, the noise level is about 100 G, so areas where the transverse component of magnetic field is more than 200 G (2σ) are selected.

2.1.2. Parameters and Calculating Methods of Current Helicity

Two parameters are used in this work to quantify the helicity patterns. They are the force-free field coefficient α (Pevtsov, Canfield, and Metcalf, 1995; Hagyard and Pevtsov, 1999) and the current helicity component h_c (Abramenko, Wang, and Yurchyshyn, 1996; Bao and Zhang, 1998). Both of them can be directly determined from the observed vector magnetograms.

Force-Free Field Factor α_{best}: The constant-α force-free calculation uses the normal component of the photospheric field B_z as the boundary condition. According to the force-free equation $\bigtriangledown \times \mathbf{B} = \alpha \mathbf{B}$, we calculate the value of the proxy α that gives the best match between the calculated and observed horizontal field components, B_x and B_y, in the sense of a minimum least-squares difference. When the parameter α is varied, the least-squares differences are also changed following the value of α. Once the minimum value of the least-squares differences is determined, the value of α at the minimum, called α_{best}, can be expressed by using the following formula:

$$\frac{\sum [B_{cal}(\alpha_{best}) - B_{obs}]^2}{\sum B^2} = \min . \tag{4}$$

The Local Current Helicity h_c: The local current helicity is defined as

$$h_c = \mu B_z J_z, \tag{5}$$

where B_z is the vertical component of the magnetic field and J_z is the vertical electric current from the observed azimuthal magnetic field. In our calculation, the local current helicity per active region always contains a mixture of positive and negative helicity. To reveal whether a predominant sign exists, we calculate the quantity ρ_h, which is defined as

$$\rho_h = \frac{\sum h_c(i, j)}{\sum |h_c(i, j)|}, \tag{6}$$

where $\sum$ represents the sum of a whole active region and $h_c(i, j)$ is the value of current helicity in a given pixel (i, j). The quantity ρ_h is called the imbalance of current helicity over an active region and describes the ratio of net to total unsigned helicity density. From the equation, we can deduce that ρ_h has the same sign as $\sum h_c$.

2.1.3. Data Reduction

The vector magnetic field data having favorable seeing conditions and within $\pm 35^\circ$ longitude from the disk center are included. A total of 43 pairs of active regions connected by TLs are covered by about 800 vector magnetograms satisfying these conditions. Since more than one TL may originate from an active region forming transequatorial connections with more than one other active region, there are 50 pairs of magnetic polarity regions, and the sample of 43 pairs of active regions, in fact, consists of 81 active regions. Based on the two parameters, we calculate the average helicity value of every active region and the mean current helicity of the magnetic polarity regions.

2.2. Extrapolation

The twist signs of the transequatorial loops deduced from the extrapolation are more reliable than those derived visually from the morphological structures. Using the method of Chiu and Hilton (1977), we make force-free field extrapolations for these TLs, which assumes that the corona magnetic field is a constant-α force-free field and solves the linear force-free field equation, using Green's function techniques. In this study, we consider the solar surface as spherical, making projection correction for each magnetogram, then the derived longitudinal magnetic field on the photospheric surface is taken as a boundary condition.

The longitudinal magnetic field data are obtained from the SOHO Michelson and Doppler Instrument (MDI) first; if there are no corresponding data, these are replaced by data from the National Solar Observatory at Kitt Peak. We calculate the magnetic field line in the corona using the extrapolation code, changing the α value continuously. Extrapolated field lines that best fit the TL configuration observed in *Yohkoh* soft X rays give the needed α value.

3. Results

3.1. An Example

To clearly demonstrate how we select and deal with the data and what methods we use, an example is presented. Figure 1a is a *Yohkoh* soft X-ray image on 19 January 1999 which shows a transequatorial loop in the corona. Figure 1b shows the corresponding Kitt Peak full-disk longitudinal magnetogram. From the figures we can see that the transequatorial loop connected the positive magnetic polarity of AR 8440 in the northern hemisphere and another footpoint existed in the negative polarity region of AR 8439 in the southern hemisphere. The corresponding vector magnetograms of the two active regions at HSOS are then found.

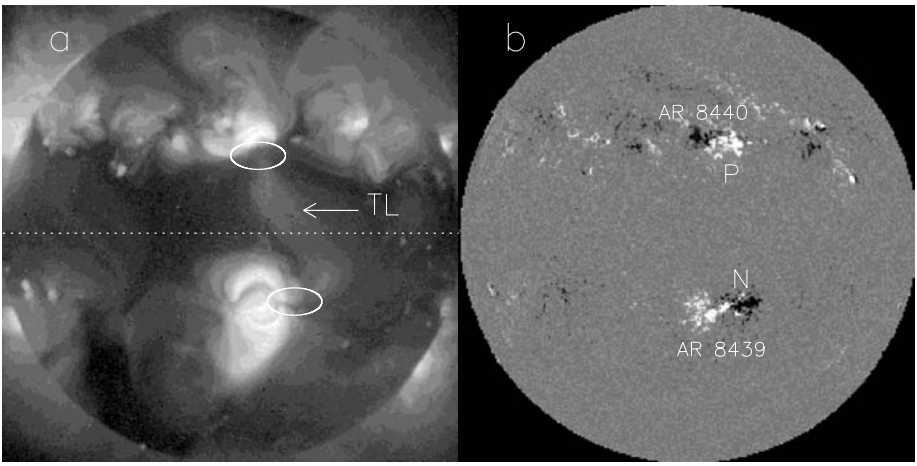

Figure 1 (a) A *Yohkoh* soft X-ray image presents a transequatorial loop on 19 January 1999. The two *ellipses* indicate the regions that the transequatorial loop connected. (b) Corresponding Kitt Peak full-disk longitudinal magnetogram. 'P' represents the positive magnetic polarity and 'N' shows the negative magnetic polarity footpoints of the TL.

Table 1 The helicity values of AR 8440 and AR 8439.

AR number	$\alpha_{\rm best}$	ρ_h	$\alpha_{\rm best}$ (MP)	ρ_h (MP)
8440	1.16	31%	1.17(P)	29%(P)
8439	0.04	21%	0.79(N)	11%(N)

Note. The units of $\alpha_{\rm best}$ are 10^{-8} m^{-1}. 'MP' represents the magnetic polarity regions; 'P' shows the positive magnetic polarity region and 'N' shows the negative magnetic polarity region.

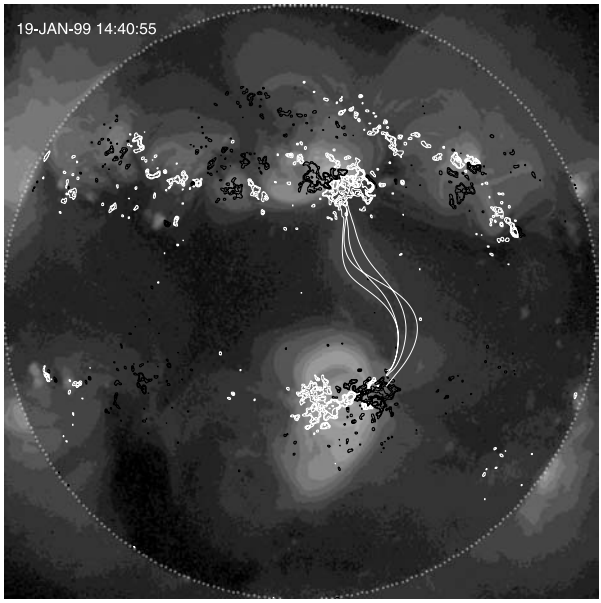

Figure 2 Linear force-free field extrapolation of a transequatorial loop connecting two active regions ($\alpha = 1.7 \times 10^{-3}$ Mm^{-1}). The gray-scale image is the *Yohkoh* soft X-ray observation; the contour shows a Kitt Peak magnetogram at 16:56:34 UT. White (black) contours represent positive (negative) magnetic field.

We select the magnetograms with good seeing conditions and near the central meridian; they are handled according to the processes described in Section 2.1. We calculate the mean values of $\alpha_{\rm best}$ and ρ_h of the two active regions, and find their signs positive. Then we compute the average current helicity values of the positive magnetic polarity region of AR 8440 and the negative magnetic polarity region of AR 8439. The current helicity values of the active regions and the magnetic polarity regions are exhibited in Table 1. The results show that the pair of active regions (AR 8440, AR 8439) have the same chirality and the pair of magnetic polarity regions connected by this TL also have the same handedness.

Figure 2 shows the distribution of magnetic field lines of a transequatorial loop in the corona. The magnetic field lines are extrapolated through the method introduced in Section 2.2. They are calculated by the approximation of a constant-α force-free magnetic field and the α value is 1.7×10^{-3} Mm^{-1}. The results indicate that the sign of twist in the TL is the same as that of the magnetic polarities connected by the TL.

3.2. Statistical Results

The chirality relation of the active region pairs and the helicity pattern relation of the magnetic polarity pairs connected by the TLs are analyzed. The statistical results are demon-

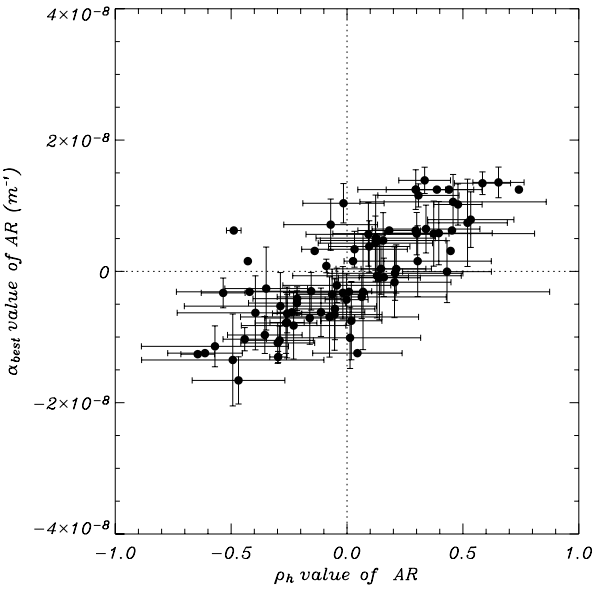

Figure 3 Relationship between ρ_h and α_{best} of the active regions. Error bars (when present) correspond to 1σ of the mean helicity values from multiple magnetograms of the same active region. Points without error bars correspond to active regions represented by a single magnetogram.

strated in the following subsections. The linear force-free α parameter values of TLs are also computed.

3.2.1. Relationship between the Two Parameters

In this part, we investigate the correlation of the two parameters (α_{best} and ρ_h) that characterize the current helicity of the active regions and magnetic polarity regions. Figure 3 shows the relations between these two parameters when calculating the current helicity of the active regions, demonstrating good correspondence. Among the selected 81 active regions, 63 (78%) active regions have the same sign. For the active regions for which the two parameters have opposite signs, most of them have small helicity values and the standard deviation (1σ) is larger than the average value. Figure 4 shows the correlation of the two parameters when computing the current helicity of the magnetic polarities regions: 90% of the regions show the same sign. The reason for the higher correlation of helicity for the two parameters of the magnetic polarity regions than for the active regions may be because both positive and negative helicity patches are present within a sunspot. By averaging this pattern, one can get a near-zero value, which might be slightly negative or positive. Among 81 active regions, there are 20 cases for which ρ_h values are less than 0.1. If we remove these cases, the correlation between the two parameters in the active regions will increase to 85%.

3.2.2. Chirality Relationship of the Active Region Pairs

Figure 5 exhibits the helicity relationship of the 43 pairs of active regions connected by transequatorial loops; it does not show an obvious correlation between them. For the parameter α_{best}, 22 pairs (51%) of active regions have the same sign of current helicity and 21 pairs (49%) have opposite sign. Applying the parameter ρ_h, we obtain 26 pairs (60%) of active regions showing the same sign and 17 pairs (40%) showing opposite sign.

For the 81 active regions, in 10 cases the α_{best} values are less than 2×10^{-9} m^{-1} and the standard deviation (1σ) is more than the mean value. If we remove these regions, 33 pairs

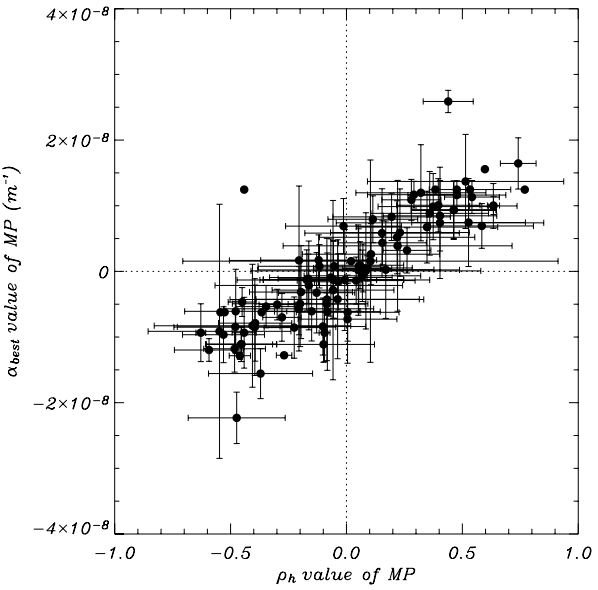

Figure 4 Relationship between ρ_h and $\alpha_{\rm best}$ of the magnetic polarity regions. Error bars (when present) correspond to 1σ of the mean helicity values from multiple magnetograms of the same magnetic polarity region. Points without error bars correspond to magnetic polarity regions represented by a single magnetogram.

of active regions are left. Among these pairs, in 17 (52%) pairs of active regions the signs of $\alpha_{\rm best}$ are the same and 18 (55%) pairs have the same sign for ρ_h. If we also subtract the pairs for which only one magnetogram is available for one or two regions, only 25 pairs are left. There are 14 (56%) pairs showing the same sign for $\alpha_{\rm best}$ and 15 (60%) pairs carrying the same sign for ρ_h.

These results demonstrate that only slightly more than half of the active region pairs connected by transequatorial loops have the same signs of current helicity.

Pevtsov (2000) classified transequatorial loops into 'connection' and 'reconnection' types according to configuration. He calculated 22 pairs of active regions using $\alpha_{\rm best}$; 14 cases are included in the 'connection' type and 8 cases are included in the 'reconnection' type. For the 'connection' cases, 50% of the active region pairs have the same sign; for the 'reconnection' cases, all the active region pairs had the same sign. Based on the method of Pevtsov, 26 of our TL cases belong to the 'connection' type and 17 cases belong to the 'reconnection' type for the selected 43 TLs. In 10 active region pairs the signs of current helicity are the same for the 'connection' type (38%), whereas 12 (71%) of active region pairs have the same helicity signs for the 'reconnection' type. The two results show that the 'reconnection' type transequatorial loops tend to have the same chirality in both active regions.

3.2.3. Hemispheric Rule of the Chirality

The selected active regions include regions of solar cycles 22 and 23. To verify whether there is any correlation of the chirality of active region pairs connected by TLs, we consider the hemispheric rule of these active regions. Figures 6a and 6b show the latitudinal distribution of the current helicity of the total active regions. We observe that the active regions connected by TLs follow the hemispheric helicity rule found earlier for other active region samples. For $\alpha_{\rm best}$, 68% (28) of the 41 active regions in the northern hemisphere show $\alpha_{\rm best} < 0$ and 60% (24) of the 40 active regions in the southern hemisphere show $\alpha_{\rm best} > 0$;

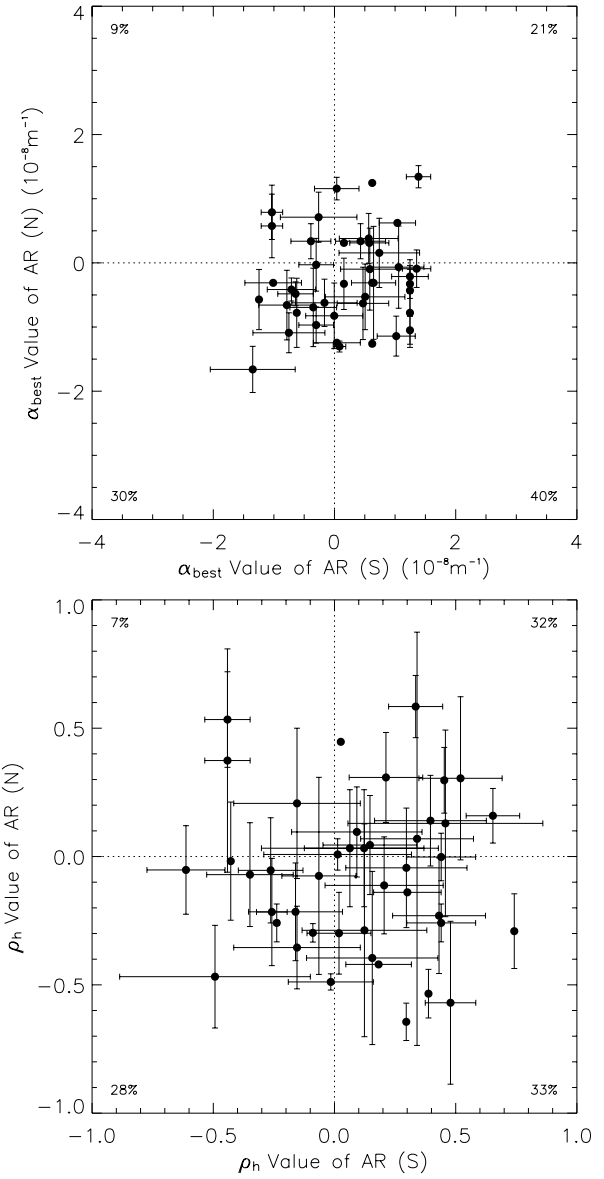

Figure 5 Top: Correlation of α_{best} of the active region pairs connected by TLs. Bottom: Relationship of ρ_h of the active region pairs connected by TLs. The abscissa axis presents the helicity values of active regions in the southern hemisphere; the ordinate axis shows the values in the northern hemisphere. Other symbols are the same as in Figure 3.

for the imbalance ρ_h of helicity, 59% of the active regions in the northern hemisphere show $\rho_h < 0$ and 65% of the active regions in the southern hemisphere show $\rho_h > 0$.

Not only does the whole data set show the hemispheric rule, but also do the active regions within an individual solar cycle. In solar cycle 22 (Figures 6c and 6d), for α_{best}, 60% of the active regions in the northern hemisphere show $\alpha_{best} < 0$ and 72% of the active regions in the southern hemisphere show $\alpha_{best} > 0$; for the imbalance ρ_h of helicity, 70% of the active regions in the northern hemisphere show $\rho_h < 0$ and 72% of the active regions in the southern hemisphere show $\rho_h > 0$. These results are consistent with the results of previous

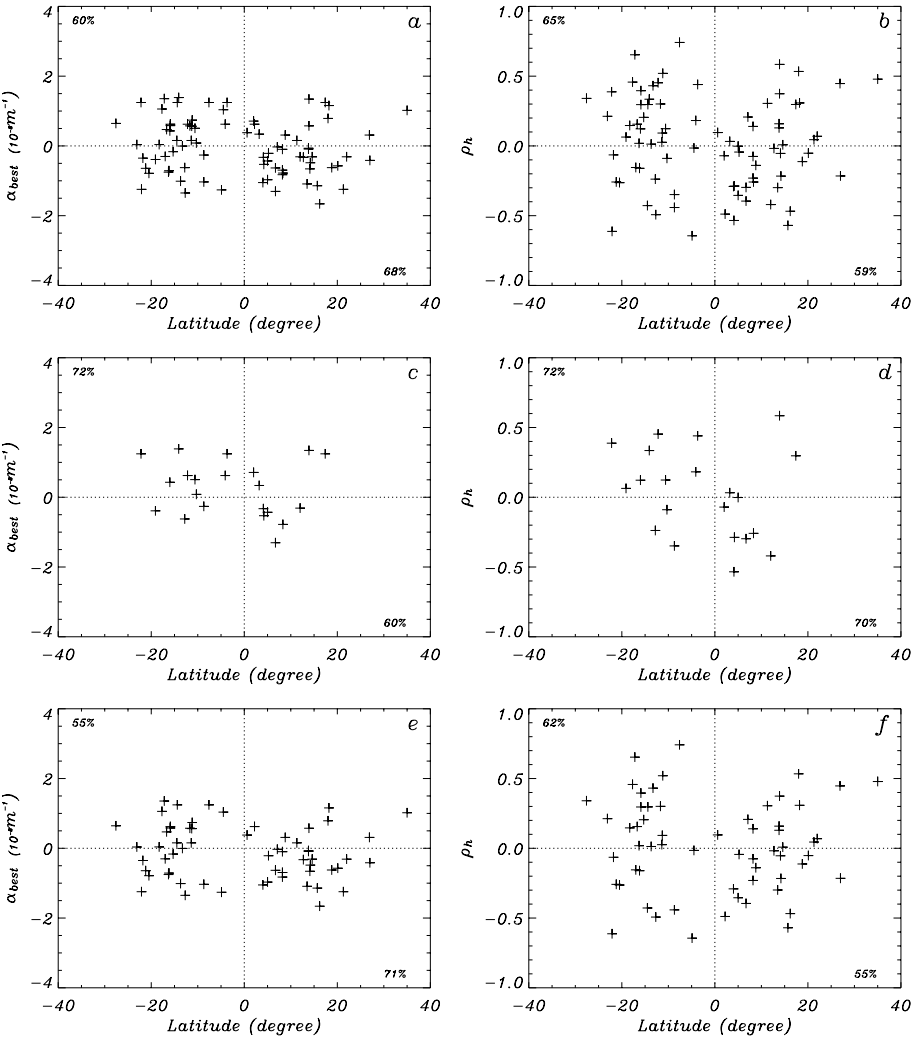

Figure 6 Latitudinal distribution of α_{best} and ρ_h. (a) Latitudinal distribution of α_{best} for all the selected active regions. (b) Latitudinal distribution of ρ_h for all the selected active regions. (c) and (e) Latitudinal distribution of α_{best} for the selected active regions in solar cycles 22 and 23, respectively. (d) and (f) Latitudinal distribution of ρ_h for the selected active regions in solar cycles 22 and 23, respectively.

investigations (Pevtsov, Canfield, and Metcalf, 1995; Bao and Zhang, 1998). In solar cycle 23 (Figures 6e and 6f), for α_{best}, 71% of the active regions in the northern hemisphere show $\alpha_{\text{best}} < 0$ and 55% of the active regions in the southern hemisphere show $\alpha_{\text{best}} > 0$; for the imbalance ρ_h of helicity, 55% of the active regions in the northern hemisphere show $\rho_h < 0$ and 62% of the active regions in the southern hemisphere show $\rho_h > 0$. These results are consistent with previous research findings (Pevtsov, Canfield, and Latushko, 2001; Zhang, 2006).

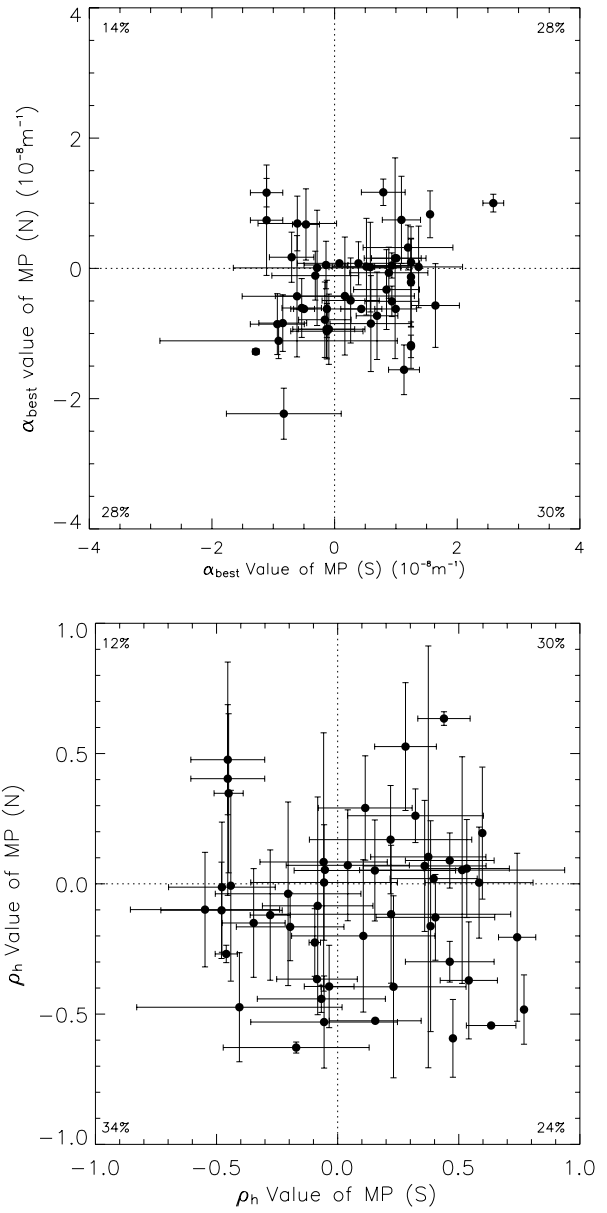

Figure 7 Top: Correlation of α_{best} of the magnetic polarity pairs connected by TLs. Bottom: Relationship of ρ_h of the magnetic polarity pairs connected by TLs. The abscissa axis presents the helicity values of magnetic polarity regions in the southern hemisphere; the ordinate axis shows the values in the northern hemisphere. Other symbol are the same as in Figure 4.

3.2.4. Helicity Relation of the Magnetic Polarity Pairs

Figure 7 presents the helicity relation of 50 pairs of the magnetic polarity regions connected by TLs. The top panel shows the correlation of the magnetic polarity regions based on the parameter α_{best}: 28 pairs (56%) show the same helicity signs and 22 pairs (44%) show the opposite. The bottom panel gives the correlation using the parameter ρ_h: 32 pairs (64%) exhibit the same handedness and 18 pairs (36%) exhibit the opposite.

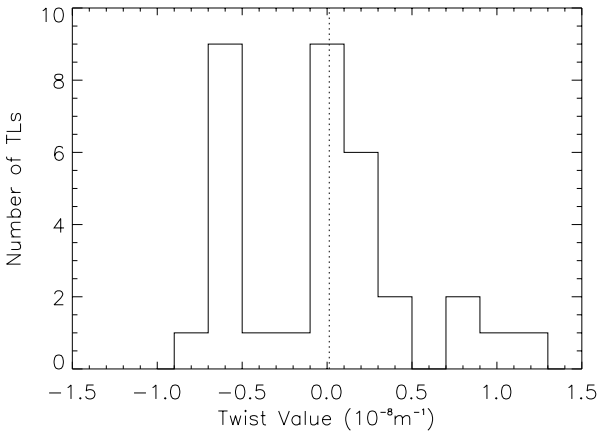

Figure 8 Distribution of the linear force-free α parameter (twist) values of TLs. The dotted line shows the average value.

Table 2 Relationship between the TL extrapolation signs and helicity patterns of the footpoints pairs.

Proxy	α_{best}						
Helicity relation of footpoints	Same			Opposite			
Relation between TLs	Same	Opposite	Potential (TL)	TL sign	Positive	Negative	Potential
Twist and helicity of footpoints	12	4	3	Number	7	5	2

3.2.5. Twist of the Transequatorial Loops

Based on the observed longitudinal magnetic field, we extrapolate the selected transequatorial loops. Some TLs have no corresponding full-disk magnetograms and for some TLs we were unable to establish a definite sign through fitting extrapolated field lines to a soft X-ray image; therefore only 33 TLs are extrapolated. The distribution of TL numbers for different twist values are presented in Figure 8. In 16 TL cases the signs of the linear force-free α parameter (twist signs) are positive, 12 TLs have negative twist signs, and 5 TLs have extrapolated values of zero. From the figure, we can obtain that the average value is close to 0.

The TLs are extrapolated by using the linear force-free field model and the parameters α_{best} characterizing the photospheric current helicity, which are derived from the force-free field equation. These two quantities are comparable. For ρ_h, although it can represent the current helicity at a certain degree, however, it expresses a different physical meaning to the extrapolation value. Therefore, we analyze the relationship between the extrapolated value of TL and α_{best}. Being a magnetic structure, a TL connects opposite magnetic polarities; the helicity relationship between the TLs and the magnetic polarity region pairs have to be considered. These TLs are divided into two groups according to whether their footpoints have the same sign of α_{best}. There are 19 TLs for which the footpoints pairs show the same sign of α_{best} and 14 TLs for which the footpoints pairs show different signs. For the first group, 12 TLs show the same twist signs as the footpoints regions; 4 TLs show opposite signs to that in the footpoint regions. For the second group, there are 7 TLs having positive sign and 5 TLs with a negative twist. These results are listed in Table 2, which shows that the twist of the TLs has a tendency for having the same sign as the current helicity of footpoints pairs.

4. Discussion and Conclusions

The helicity signs of 43 pairs of active regions connected by TLs are computed: About 51% of the active region pairs show the same chirality if one uses $\alpha_{\rm best}$, and 60% of the active region pairs demonstrate the same handedness, when one uses ρ_h. Further, we calculate 50 pairs of magnetic polarity regions connected by the TLs: About 56% of the magnetic polarity region pairs show the same chirality, if one uses $\alpha_{\rm best}$, and 64% of the magnetic polarity region pairs demonstrate the same handedness, when one uses ρ_h. These result do not support a tendency for transequatorial loops to connect two regions having the same handedness, which may be caused by helicity cancelation of mixed footpoint helicity signs.

Pevtsov (2000) used the *Yohkoh* soft X-ray data set from 1991 to 1998 and found 22 active region pairs connected by transequatorial loops. In these cases, 68% of the active region pairs have the same chirality. We extend the data to a larger number of active regions, analyzing 43 pairs of active regions. Using the same parameter force-free factor $\alpha_{\rm best}$ as Pevtsov (2000), we find that in 22 cases (51%) both active regions have the same signs of current helicity, and in 21 cases (49%) the regions have opposite signs. Several reasons can lead to the different results. First, Pevtsov (2000) selected the magnetograms from the Haleakala Stokes Polarimeter (HSP) whereas we obtain them from the Solar Magnetic Field Telescope (SMFT), and there is some difference between the two instruments. Although Pevtsov, Dun, and Zhang (2006) found that there is a good correlation between SMFT and HSP data in about 80% of cases in the same sign of $\alpha_{\rm best}$, some slight difference also exists in about 20% of the cases carrying the opposite sign of $\alpha_{\rm best}$. If we consider the relation of the active region pairs, the correlation will be less than 80%. Second, the active regions selected are different, and different samples lead to different results. Moreover, Pevtsov (2000) found that about 68% of the active region pairs connected by transequatorial loops tend to have the same handedness, but the rule is weak. Finally, both of us use small data sets, which can also induce differing results. To demonstrate the possible effect of a small data set, one can consider the first 19 entries in Tables 3 and 4 in the Appendix. In this subset, only 6 (32%) out of 19 active region pairs have the same sign of $\alpha_{\rm best}$. However, the result is different when one uses ρ_h: 12 (63%) out of 19 active regions have the same helicity. We therefore advocate further investigations using data sets of different instruments and using very large data sets.

There is a slight difference between the two parameters ($\alpha_{\rm best}$, ρ_h) when we calculate the photospheric current helicity, because the two parameters demonstrate different physical meaning (Hagyard and Pevtsov, 1999) and there are different observational results in other studies (Pevtsov, Canfield, and Metcalf, 1995; Pevtsov, Canfield, and Latushko, 2001; Bao and Zhang, 1998; Zhang, 2006). However, we find good correlation between them.

Although the selected active regions are joined by the TLs, they also obey the hemispheric rule in solar cycles 22 and 23, respectively. The hemispheric rule of the active regions certify that helicity patterns of the active region pairs connected by TLs have no obvious correlation.

All the selected transequatorial loops are classified into 'reconnection' and 'connection' types. For the 'reconnection' category, about 71% of active region pairs have the same current helicity sign, which is the same tendency as found by Pevtsov (2000).

The twist values of 33 transequatorial loops are inferred through the force-free field extrapolation. In 16 cases the TLs twist values are positive and 12 cases have negative values. This finding matches that of Rust and Kumar (1996): For 23 transequatorial soft X-ray loops, the number of forward-S shaped loops are almost equal to the reverse-S shaped ones (12 versus 11). Then the relationship between the twist of TLs and the helicity patterns of

their footpoint regions are analyzed. There are 12 cases for which the twist signs of the TLs are the same as the helicity signs of the footpoint pairs whereas in 4 cases it is found to be opposite. This indicates that the twists of the TLs tend to show the same signs as the footpoint pairs.

Acknowledgements The authors would like to thank the anonymous referee for valuable suggestions and Lidia van Driel-Gesztelyi for her helpful comments that helped in improving the manuscript. J. Chen gratefully thanks Yuanyong Deng, Mei Zhang, Jihong Liu, Yu Gao, Jiangtao Su, and Yin Zhang for their discussions and we also thank the other members of the Huairou Observing Station for their instruction and encouragement. This study is supported by Grant Nos. 10373016, 10233050, 10228307, 10611120338, and 10473016 of the National Natural Science Foundation of China and TG 2000078401 and 2006CB806301 of the National Basic Research Program of China. NSO/Kitt Peak data used are produced cooperatively by NSF/NOAO, NASA/GSFC, and NOAA/SEL. SOHO is a project of international cooperation between ESA and NASA, and *Yohkoh* is a mission of ISAS (Japan) with participation from the United States and the United Kingdom.

Appendix

Tables 3 and 4 present the mean helicity values of the active regions and the opposite magnetic polarity regions connected by TLs using α_{best} and ρ_h, respectively. In Table 3, column 1 gives the dates of soft X-ray images with transequatorial loops. Column 2 presents the hemisphere in which the active regions existed, with 'N' denoting the northern hemisphere and 'S' the southern hemisphere. Column 3 exhibits the active region number of NOAA. The average helicity values and 1σ error values of the corresponding active regions are shown in column 4, and column 5 shows the magnetic polarity connected by the TL, with 'N' representing negative magnetic polarity and 'P' positive polarity. The mean helicity values and 1σ error values of the magnetic polarity regions corresponding to column 5 are presented in column 6. Note that there may be more than one TL connecting two ARs and one AR may be connected to more than one AR via TLs. Column 7 shows the other magnetic polarity pairs connected by another TL. The mean helicity values and the error values of the magnetic polarity regions corresponding to column 7 are listed in column 8.

Table 3 The α_{best} value of the region pairs connected by transequatorial loops.

Date	Hemisphere	NOAA AR	α_{best} (AR)	MP	α_{best} (MP)	MP	α_{best} (MP)
28 Oct. 1991	S	6891	1.39 ± 0.20	P	1.09 ± 0.31	N	2.59 ± 0.17
	N	6893	1.34 ± 0.17	N	0.74 ± 0.67	P	1.00 ± 0.14
07 Jan. 1992	S	6993	0.08 ± 0.10	P	-1.28 ± 0.06		
	N	6996	-1.30 ± 0.08	N	-1.28 ± 0.04		
20 Jan. 1992	S	7012	0.62 ± 0.00	P	1.56 ± 0.00		
	N	7019	1.24 ± 0.00	N	0.83 ± 0.36		
27 Feb. 1992	N	7067	-0.43 ± 0.39	N	0.04 ± 0.19		
	S	7069	1.25 ± 0.00	P	0.93 ± 0.44		
	S	7069	1.25 ± 0.00	P	0.93 ± 0.44		
	N	7070	-0.78 ± 0.54	N	-0.51 ± 0.23		
	N	7070	-0.78 ± 0.54	P	-0.86 ± 0.47		
	S	7072	-0.62 ± 0.00	N	-0.93 ± 0.44		

Table 3 (*Continued.*)

Date	Hemisphere	NOAA AR	α_{best} (AR)	MP	α_{best} (MP)	MP	α_{best} (MP)
18 Apr. 1992	S	7128	0.43 ± 0.41	P	0.26 ± 0.47		
	N	7131	0.34 ± 0.27	N	-0.49 ± 0.65		
	N	7131	0.34 ± 0.27	P	0.67 ± 0.55		
	S	7130	-0.39 ± 0.33	N	-0.47 ± 0.22		
05 Jan. 1994	N	7645	0.71 ± 0.39	N	0.69 ± 0.42	P	-0.11 ± 0.38
	S	7646	-0.26 ± 0.63	P	-0.61 ± 0.64	N	-0.31 ± 0.71
24 Jan. 1995	S	7829	1.25 ± 0.00	P	1.25 ± 0.00		
	N	7830	-0.33 ± 0.23	N	-1.20 ± 0.17		
17 Apr. 1995	S	7863	0.62 ± 0.00	P	1.00 ± 0.34	N	-0.50 ± 0.17
	N	7864	-0.31 ± 0.00	N	-0.62 ± 0.00	P	-0.62 ± 0.00
25 Aug. 1995	N	7901	-0.53 ± 0.51	P	0.008 ± 0.89		
	S	7902	0.51 ± 0.66	N	-0.29 ± 1.37		
17 Dec. 1996	N	8004	-1.26 ± 0.03	P	-0.21 ± 0.68		
	S	8005	0.62 ± 0.00	N	1.25 ± 0.00		
10 Sep. 1997	N	8084	-0.31 ± 0.88	P	0.16 ± 1.54		
	S	8085	0.64 ± 0.36	N	0.99 ± 0.50		
26 Dec. 1997	S	8124	1.02 ± 0.31	P	1.13 ± 0.25		
	N	8126	-1.14 ± 0.31	N	-1.56 ± 0.38		
02 Jul. 1998	S	8258	0.16 ± 0.00	N	0.08 ± 0.00		
	N	8259	0.31 ± 0.00	P	0.08 ± 0.00		
06 Jul. 1998	S	8263	1.06 ± 0.42	N	1.37 ± 0.72		
	N	8264	-0.07 ± 0.64	P	0.02 ± 0.63		
30 Nov. 1998	S	8393	0.04 ± 0.39	N	-0.14 ± 0.36		
	N	8395	-1.25 ± 0.00	P	0.05 ± 0.36		
09 Dec. 1998	N	8402	-0.57 ± 0.47	P	-0.84 ± 0.43		
	S	8404	-1.25 ± 0.00	N	-0.85 ± 0.39		
19 Jan. 1999	S	8439	0.04 ± 0.37	N	0.79 ± 0.36		
	N	8440	1.16 ± 0.18	P	1.17 ± 0.20		
13 Feb. 1999	N	8457	-0.48 ± 0.19	P	0.17 ± 0.38		
	S	8458	-0.64 ± 0.29	N	-0.70 ± 0.36		
05 Jun. 1999	N	8558	-1.09 ± 0.31	P	-0.79 ± 0.58		
	S	8562	-0.75 ± 0.59	N	-0.16 ± 0.43		
28 Jun. 1999	S	8603	-0.17 ± 0.54	P	0.17 ± 1.13	N	0.85 ± 0.54
	N	8602	-0.62 ± 0.37	N	-0.42 ± 0.91	P	-0.33 ± 0.61
13 Jul. 1999	S	8627	-1.01 ± 0.47	N	0.39 ± 1.00		
	N	8628	-0.31 ± 0.00	P	0.08 ± 0.33		
18 Nov. 1999	S	8765	-1.03 ± 0.18	N	-1.11 ± 0.26		
	N	8766	0.79 ± 0.42	P	1.16 ± 0.22		

Table 3 (*Continued.*)

Date	Hemisphere	NOAA AR	$\alpha_{\rm best}$ (AR)	MP	$\alpha_{\rm best}$ (MP)	MP	$\alpha_{\rm best}$ (MP)
	S	8765	-1.03 ± 0.18	N	-1.11 ± 0.26		
	N	8768	0.58 ± 0.50	P	0.74 ± 0.85		
19 Jan. 2000	S	8831	-0.79 ± 0.46	N	-0.54 ± 0.32		
	N	8829	-0.66 ± 0.54	P	-0.61 ± 0.45		
26 Feb. 2000	S	8882	0.58 ± 0.48	N	0.52 ± 0.56		
	N	8883	-0.10 ± 0.64	P	0.03 ± 0.74		
09 Mar. 2000	S	8898	-0.71 ± 0.40	P	-0.09 ± 0.59		
	N	8904	-0.42 ± 0.18	N	-0.93 ± 0.54		
20 Apr. 2000	N	8963	-1.66 ± 0.36	P	-2.23 ± 0.39		
	S	8968	-1.35 ± 0.70	N	-0.83 ± 0.94		
28 Apr. 2000	S	8970	1.36 ± 0.23	P	1.20 ± 0.73	N	1.64 ± 0.39
	N	8971	-0.09 ± 0.29	N	0.32 ± 0.34	P	-0.57 ± 0.64
27 Jun. 2000	N	9054	0.16 ± 0.54	P	0.09 ± 0.36		
	S	9056	0.74 ± 0.67	N	1.25 ± 0.00		
22 Jul. 2000	N	9097	-1.05 ± 0.22	P	-1.18 ± 0.36		
	S	9096	1.25 ± 0.00	N	1.25 ± 0.00		
29 Aug. 2000	N	9140	-0.21 ± 0.26	P	-0.07 ± 0.39		
	S	9143	1.25 ± 0.30	N	0.88 ± 0.64		
05 Sep. 2000	N	9147	-0.63 ± 0.56	P	-0.85 ± 0.74		
	S	9154	0.47 ± 0.42	N	0.59 ± 0.67		
29 Sep. 2000	S	9173	0.57 ± 0.32	P	0.44 ± 0.34	N	1.01 ± 0.41
	N	9172	0.31 ± 0.00	N	-0.62 ± 0.00	P	0.16 ± 0.00
02 Nov. 2000	S	9214	0.56 ± 0.48	N	0.58 ± 0.68		
	N	9213	0.38 ± 0.39	P	0.02 ± 0.69		
20 Dec. 2000	N	9278	-0.03 ± 0.41	P	-0.62 ± 0.44		
	S	9279	-0.30 ± 0.29	N	-0.13 ± 0.59		
23 Dec. 2000	S	9279	-0.30 ± 0.29	P	-0.91 ± 1.94	N	-0.13 ± 0.59
	N	9280	-0.97 ± 0.28	N	-1.11 ± 0.27	P	-0.96 ± 0.43
09 Jan. 2001	N	9296	-0.69 ± 0.61	P	-0.43 ± 0.93		
	S	9295	-0.35 ± 0.39	N	-0.61 ± 0.89		
09 Feb. 2001	N	9335	-0.83 ± 0.51	P	-0.73 ± 0.67		
	S	9339	-0.004 ± 0.47	N	0.69 ± 0.34		
26 Feb. 2001	N	9359	-0.33 ± 0.40	P	-0.13 ± 0.77		
	S	9360	0.16 ± 0.00	N	1.25 ± 0.00		
15 Mar. 2001	S	9373	1.04 ± 0.30	N	-0.13 ± 0.46		
	N	9384	0.62 ± 0.00	P	-0.93 ± 0.44		

Note. The units of $\alpha_{\rm best}$ are 10^{-8} m^{-1}. The error value is the 1σ level. 'MP' represents the magnetic polarity regions; 'P' shows positive magnetic polarity and 'N' negative magnetic polarity.

Table 4 The ρ_h value of the region pairs connected by transequatorial loops.

Date	Hemisphere	NOAA AR	ρ_h (AR)	MP	ρ_h (MP)	MP	ρ_h (MP)
28 Oct. 1991	S	6891	0.33 ± 0.11	P	0.28 ± 0.13	N	0.44 ± 0.11
	N	6893	0.58 ± 0.12	N	0.53 ± 0.25	P	0.63 ± 0.03
07 Jan. 1992	S	6993	-0.09 ± 0.00	P	-0.46 ± 0.05		
	N	6996	-0.30 ± 0.04	N	-0.27 ± 0.03		
20 Jan. 1992	S	7012	0.45 ± 0.00	P	0.60 ± 0.00		
	N	7019	0.30 ± 0.13	N	0.19 ± 0.25		
27 Feb. 1992	N	7067	-0.002 ± 0.09	N	0.09 ± 0.11		
	S	7069	0.44 ± 0.14	P	0.46 ± 0.18		
	S	7069	0.44 ± 0.14	P	0.46 ± 0.18		
	N	7070	-0.26 ± 0.07	N	-0.30 ± 0.08		
	N	7070	-0.26 ± 0.07	P	-0.23 ± 0.13		
	S	7072	-0.24 ± 0.01	N	-0.09 ± 0.02		
18 Apr. 1992	S	7128	0.12 ± 0.25	P	0.11 ± 0.30		
	N	7131	0.03 ± 0.23	N	-0.20 ± 0.29		
	N	7131	0.03 ± 0.23	P	0.35 ± 0.31		
	S	7130	0.06 ± 0.36	N	-0.45 ± 0.06		
05 Jan. 1994	N	7645	-0.07 ± 0.20	N	-0.01 ± 0.25	P	-0.17 ± 0.13
	S	7646	-0.35 ± 0.18	P	-0.48 ± 0.22	N	-0.20 ± 0.22
24 Jan. 1995	S	7829	0.39 ± 0.00	P	0.48 ± 0.00		
	N	7830	-0.53 ± 0.09	N	-0.59 ± 0.15		
17 Apr. 1995	S	7863	0.18 ± 0.14	P	0.63 ± 0.10	N	-0.09 ± 0.17
	N	7864	-0.42 ± 0.00	N	-0.54 ± 0.00	P	-0.37 ± 0.00
25 Aug. 1995	N	7901	-0.29 ± 0.41	P	0.08 ± 0.50		
	S	7902	0.12 ± 0.26	N	-0.06 ± 0.26		
17 Dec. 1996	N	8004	-0.64 ± 0.07	P	-0.16 ± 0.40		
	S	8005	0.30 ± 0.00	N	0.38 ± 0.00		
10 Sep. 1997	N	8084	0.07 ± 0.81	P	0.10 ± 0.81		
	S	8085	0.34 ± 0.23	N	0.37 ± 0.24		
26 Dec. 1997	S	8124	0.48 ± 0.10	P	0.54 ± 0.12		
	N	8126	-0.57 ± 0.32	N	-0.37 ± 0.22		
02 Jul. 1998	S	8258	0.03 ± 0.00	N	-0.05 ± 0.00		
	N	8259	0.45 ± 0.00	P	0.05 ± 0.00		
06 Jul. 1998	S	8263	0.46 ± 0.40	N	0.51 ± 0.42		
	N	8264	0.13 ± 0.36	P	0.05 ± 0.43		
30 Nov. 1998	S	8393	0.15 ± 0.19	N	0.04 ± 0.25		
	N	8395	0.04 ± 0.19	P	0.07 ± 0.21		
09 Dec. 1998	N	8402	-0.05 ± 0.17	P	-0.10 ± 0.18		
	S	8404	-0.61 ± 0.16	N	-0.48 ± 0.25		

Table 4 (*Continued.*)

Date	Hemisphere	NOAA AR	ρ_h (AR)	MP	ρ_h (MP)	MP	ρ_h (MP)
19 Jan. 1999	S	8439	0.21 ± 0.15	N	0.11 ± 0.19		
	N	8440	0.31 ± 0.18	P	0.29 ± 0.20		
13 Feb. 1999	N	8457	-0.22 ± 0.21	P	-0.12 ± 0.25		
	S	8458	-0.26 ± 0.06	N	-0.28 ± 0.08		
05 Jun. 1999	N	8558	-0.30 ± 0.16	P	-0.39 ± 0.16		
	S	8562	0.02 ± 0.13	N	-0.04 ± 0.10		
28 Jun. 1999	S	8603	0.20 ± 0.24	P	-0.20 ± 0.30	N	0.40 ± 0.24
	N	8602	-0.11 ± 0.19	N	-0.04 ± 0.35	P	-0.13 ± 0.16
13 Jul. 1999	S	8627	0.01 ± 0.30	N	0.22 ± 0.49		
	N	8628	0.01 ± 0.06	P	-0.12 ± 0.26		
18 Nov. 1999	S	8765	-0.44 ± 0.09	N	-0.45 ± 0.15		
	N	8766	0.53 ± 0.19	P	0.48 ± 0.21		
	S	8765	-0.44 ± 0.09	N	-0.45 ± 0.15		
	N	8768	0.37 ± 0.44	P	0.40 ± 0.45		
19 Jan. 2000	S	8831	-0.26 ± 0.13	N	-0.35 ± 0.13		
	N	8829	-0.05 ± 0.20	P	-0.15 ± 0.21		
26 Feb. 2000	S	8882	0.40 ± 0.23	N	0.22 ± 0.34		
	N	8883	0.14 ± 0.18	P	0.17 ± 0.21		
09 Mar. 2000	S	8898	-0.16 ± 0.19	P	-0.07 ± 0.26		
	N	8904	-0.22 ± 0.19	N	-0.44 ± 0.05		
20 Apr. 2000	N	8963	-0.47 ± 0.20	P	-0.47 ± 0.21		
	S	8968	-0.49 ± 0.39	N	-0.41 ± 0.42		
28 Apr. 2000	S	8970	0.65 ± 0.11	P	0.32 ± 0.28	N	0.74 ± 0.08
	N	8971	0.16 ± 0.11	N	0.26 ± 0.10	P	-0.21 ± 0.32
27 Jun. 2000	N	9054	0.30 ± 0.32	P	0.06 ± 0.19		
	S	9056	0.52 ± 0.17	N	0.53 ± 0.18		
22 Jul. 2000	N	9097	-0.29 ± 0.15	P	-0.48 ± 0.13		
	S	9096	0.74 ± 0.00	N	0.77 ± 0.00		
29 Aug. 2000	N	9140	-0.04 ± 0.23	P	0.07 ± 0.25		
	S	9143	0.30 ± 0.25	N	0.36 ± 0.25		
05 Sep. 2000	N	9147	-0.40 ± 0.34	P	-0.40 ± 0.35		
	S	9154	0.16 ± 0.27	N	0.23 ± 0.30		
29 Sep. 2000	S	9173	0.30 ± 0.14	P	0.16 ± 0.19	N	0.40 ± 0.18
	N	9172	-0.14 ± 0.00	N	-0.53 ± 0.00	P	0.02 ± 0.00
02 Nov. 2000	S	9214	0.09 ± 0.27	N	0.15 ± 0.33		
	N	9213	0.10 ± 0.18	P	0.05 ± 0.19		
20 Dec. 2000	N	9278	0.21 ± 0.29	P	0.005 ± 0.22		
	S	9279	-0.15 ± 0.26	N	-0.06 ± 0.30		

Table 4 (*Continued.*)

Date	Hemisphere	NOAA AR	ρ_h (AR)	MP	ρ_h (MP)	MP	ρ_h (MP)
23 Dec. 2000	S	9279	-0.15 ± 0.26	P	-0.55 ± 0.31	N	-0.06 ± 0.30
	N	9280	-0.35 ± 0.16	N	-0.10 ± 0.22	P	-0.53 ± 0.18
09 Jan. 2001	N	9296	-0.08 ± 0.38	P	-0.08 ± 0.42		
	S	9295	-0.06 ± 0.15	N	-0.08 ± 0.23		
09 Feb. 2001	N	9335	-0.23 ± 0.23	P	0.005 ± 0.21		
	S	9339	0.43 ± 0.19	N	0.58 ± 0.22		
26 Feb. 2001	N	9359	-0.02 ± 0.23	P	-0.007 ± 0.37		
	S	9360	-0.43 ± 0.00	N	-0.44 ± 0.00		
15 Mar. 2001	S	9373	-0.02 ± 0.18	N	-0.17 ± 0.30		
	N	9384	-0.49 ± 0.03	P	-0.63 ± 0.02		

Note. The error value is the 1σ level. 'MP' represents the magnetic polarity regions; 'P' shows positive magnetic polarity and 'N' negative magnetic polarity.

Table 4 gives helicity values using ρ_h, with other entries similar to those in Table 3.

Table 5 demonstrates the extrapolation values of TLs and the current helicity values of footpoint regions. Column 1 gives the dates of soft X-ray images with transequatorial loops. Column 2 presents the force-free field value α of the TL. The hemisphere of the active regions are given in column 3. Column 4 shows the active region number of the footpoint of the TL, with 'P' and 'N' denoting the magnetic polarity regions connected by the TL. Column 5 shows the α_{best} value of the footpoint regions of the TLs.

Table 5 The α value of TLs and the mean α_{best} value of the region pairs connected by transequatorial loops.

Date	α (TL)	Hemisphere	NOAA AR	α_{best}
28 Oct. 1991	0.17	S	6891 (N)	2.59
		N	6893 (P)	1.00
07 Jan. 1992	−0.87	S	6993 (P)	−1.28
		N	6996 (N)	−1.28
05 Jan. 1994	0.00	N	7645 (P)	−0.11
		S	7646 (N)	−0.31
	0.00	N	7645 (N)	0.69
		S	7646 (P)	−0.61
24 Jan. 1995	−0.52	S	7829 (P)	1.25
		N	7830 (N)	−1.20
25 Aug. 1995	−0.52	N	7901 (P)	0.008
		S	7902 (N)	−0.29
10 Sep. 1997	0.79	N	8084 (P)	0.16
		S	8085 (N)	0.99

Table 5 (*Continued.*)

Date	α (TL)	Hemisphere	NOAA AR	α_{best}
26 Dec. 1997	0.50	S	8124 (P)	1.13
		N	8126 (N)	−1.56
30 Nov. 1998	0.18	S	8393 (N)	−0.14
		N	8395 (P)	0.05
19 Jan. 1999	0.17	S	8439 (N)	0.79
		N	8440 (P)	1.17
13 Feb. 1999	0.79	N	8457 (P)	0.17
		S	8458 (N)	−0.70
05 Jun. 1999	0.10	N	8558 (P)	−0.79
		S	8562 (N)	−0.16
28 Jun. 1999	0.10	S	8603 (P)	0.17
		N	8602 (N)	−0.42
	0.10	S	8603 (N)	0.85
		N	8602 (P)	−0.33
13 Jul. 1999	0.20	S	8627 (N)	0.39
		N	8628 (P)	0.08
18 Nov. 1999	−0.50	S	8765 (N)	−1.11
		N	8766 (P)	1.16
	−0.50	S	8765 (N)	−1.11
		N	8768 (P)	0.74
19 Jan. 2000	0.00	S	8831 (N)	−0.54
		N	8829 (P)	−0.61
26 Feb. 2000	0.10	S	8882 (N)	0.52
		N	8883 (P)	0.03
09 Mar. 2000	1.09	S	8898 (P)	−0.09
		N	8904 (N)	−0.93
20 Apr. 2000	−0.25	N	8963 (P)	−2.23
		S	8968 (N)	−0.83
27 Jun. 2000	−0.40	N	9054 (P)	0.09
		S	9056 (N)	1.25
29 Aug. 2000	−0.50	N	9140 (P)	−0.07
		S	9143 (N)	0.88
05 Sep. 2000	0.20	N	9147 (P)	−0.85
		S	9154 (N)	0.59
29 Sep. 2000	0.50	S	9173 (N)	1.01
		N	9172 (P)	0.16
02 Nov. 2000	0.00	S	9214 (N)	0.58
		N	9213 (P)	0.02

Table 5 (*Continued.*)

Date	α (TL)	Hemisphere	NOAA AR	α_{best}
20 Dec. 2000	−0.50	N	9278 (P)	−0.62
		S	9279 (N)	−0.13
23 Dec. 2000	−0.50	S	9279 (P)	−0.91
		N	9280 (N)	−1.11
	−0.50	S	9279 (N)	−0.13
		N	9280 (P)	−0.96
09 Jan. 2001	0.20	N	9296 (P)	−0.43
		S	9295 (N)	−0.61
09 Feb. 2001	0.00	N	9335 (P)	−0.73
		S	9339 (N)	0.69
26 Feb. 2001	1.29	N	9359 (P)	−0.13
		S	9360 (N)	1.25
15 Mar. 2001	−0.50	S	9373 (N)	−0.13
		N	9384 (P)	−0.93

Note. The units of α(TL) and α_{best} are 10^{-8} m^{-1}. 'P' shows the positive magnetic polarity region and 'N' shows the negative magnetic polarity region.

References

Abramenko, V., Wang, T., Yurchyshyn, V.: 1996, *Solar Phys.* **168**, 75.
Ai, G., Hu, Y.: 1986, *Acta Astron. Sinica* **27**, 173.
Ai, G., Li, W., Zhang, H.: 1982, *Acta Astron. Sinica* **23**, 39.
Bao, S., Zhang, H.: 1998, *Astrophys. J.* **496**, 43.
Canfield, R., Pevtsov, A., McClymont, A.: 1996, In: Bentley, R.D., Mariska, J.T. (eds.) *Magnetic Reconnection in the Solar Atmosphere, ASP Conf. Ser.* **111**, 341.
Chen, J., Bao, S., Zhang, H.: 2006, *Solar Phys.* **235**, 281.
Chiu, Y., Hilton, H.: 1977, *Astrophys. J.* **212**, 873.
Fárník, M., Karlický, M., Švestka, Z.: 1999, *Solar Phys.* **187**, 33.
Fárník, M., Karlický, M., Švestka, Z.: 2001, *Solar Phys.* **202**, 81.
Hagino, M., Sakurai, T: 2004, *Publ. Astron. Soc. Japan* **56**, 831.
Hagyard, M., Pevtsov, A: 1999, *Solar Phys.* **189**, 25.
Landi Degl'Innocenti, E.: 1979, *Solar Phys.* **63**, 237.
Pevtsov, A.: 2000, *Astrophys. J.* **531**, 553.
Pevtsov, A., Canfield, R., Metcalf, T.: 1995, *Astrophys. J.* **440**, L109.
Pevtsov, A., Canfield, R., Latushko, S.: 2001, *Astrophys. J.* **549**, L261.
Pevtsov, A., Dun, J., Zhang, H.: 2006, *Solar Phys.* **234**, 203.
Rust, D., Kumar, A.: 1996, *Astrophys. J.* **464**, L199.
Sakurai, T.: 2001, In: Sigwarth, M. (ed.) *Advanced Solar Polarimetry – Theory, Observation, and Instrumentation*, *ASP Conf. Ser.* **236**, 535.
Seehafer, N.: 1990, *Solar Phys.* **125**, 219.
Su, J., Zhang, H.: 2004, *Solar Phys.* **222**, 17.
Wang, T., Ai, G., Deng, Y.: 1996, *Astrophys. Rep.* **23**, 31.
Wang, T., Xu, A., Zhang, H.: 1994, *Solar Phys.* **155**, 99.
West, E., Hagyard, M.: 1983, *Solar Phys.* **88**, 51.
Zhang, M.: 2006, *Astrophys. J.* **646**, L85.